

Research Paper

Mesoporous bioactive glass-coated 3D printed borosilicate bioactive glass scaffolds for improving repair of bone defects

Xin Qi^{1,5*}, Hui Wang^{2,6*}, Yadong Zhang^{3*}, Libin Pang^{2,6}, Wei Xiao⁴, Weitao Jia¹, Shichang Zhao^{1✉}, Deping Wang⁶, Wenhai Huang^{6✉}, Qiugen Wang⁵

1. Department of Orthopedic Surgery, Shanghai Jiao Tong University Affiliated Sixth People's Hospital, Shanghai 200233, People's Republic of China
2. Laboratory for Advanced Lubricating Materials, Shanghai Advanced Research Institute, Chinese Academy of Sciences, Shanghai 201210, China.
3. Department of Orthopedic Surgery, Shanghai Fengxian District Central Hospital, Shanghai 201400, People's Republic of China
4. Department of Materials Science and Engineering, Missouri University of Science and Technology, Rolla, MO 65409-0340, USA
5. Trauma Center, Shanghai General Hospital, School of Medicine, Shanghai Jiaotong University, Shanghai, China
6. School of Materials Science and Engineering, Tongji University, Shanghai 200092, People's Republic of China

*These authors contributed equally to this work.

✉ Corresponding authors

© Ivyspring International Publisher. This is an open access article distributed under the terms of the Creative Commons Attribution (CC BY-NC) license (<https://creativecommons.org/licenses/by-nc/4.0/>). See <http://ivyspring.com/terms> for full terms and conditions.

Received: 2017.11.15; Accepted: 2018.02.18; Published: 2018.03.28

Abstract

Background: In the field of tissue engineering, there is currently increasing interest in new biomedical materials with high osteogenic ability and comparable mechanical function to repair bone defects. Three-dimensional (3-D) bioactive borosilicate glass (BG) scaffolds exhibit uniform interconnected macro-pores, high porosity and high compressive strength. In this study, we fabricated 3-D BG scaffolds by the 3D printing technique, then coated the surface of the 3-D BG scaffolds with mesoporous bioactive glass (MBG) (BG-MBG scaffold).

Methods: The biocompatibility of the BG-MBG scaffolds was evaluated by assessing biodegradability, cell proliferation, alkaline phosphatase (ALP) activity and by quantitative reverse transcription polymerase chain reaction (qRT-PCR) analysis of osteogenic gene expression with human bone marrow stromal cells (hBMSCs). Moreover, the BG-MBG scaffolds were used to repair rat femoral defects and their performance was evaluated using microcomputed tomography (micro-CT), fluorescence labeling, histological analysis and immunohistochemical (IHC) analysis.

Results: The results showed that the BG-MBG scaffolds possessed ordered nearly 4nm meso-pores and regular macro-pores, as well as good biodegradability, and that they stimulated the proliferation and osteogenic differentiation of hBMSCs. In *in vivo* studies, the result of micro-CT reconstructed images (BG-9M group, $0.63 \pm 0.02 \text{ g/cm}^3$ and BG group $0.13 \pm 0.02 \text{ g/cm}^3$) and van Gieson staining (BG-9M groups, $62.67 \pm 3.39\%$ and BG group, $12.33 \pm 2.58\%$) showed that the BG-MBG scaffolds could significantly enhance new bone formation in both inner and peripheral scaffolds in defects, in and in without the presence of growth factors or stem cells ($P < 0.05$).

Conclusions: It is believed from these results that the BG-MBG scaffolds possess excellent osteoinductive and osteogenic properties which will make them appealing candidates for bone defect repair. The novelty of our research is to provide a new material to treat bone defects in clinic.

Key words: Borosilicate bioactive glass, Mesoporous bioactive glass, 3D printing scaffold, Bioactive coating, Osteogenesis

Introduction

In recent years, although there has been great demand for bone reconstruction of defects caused by

trauma, severe infection, tumor resection and congenital skeletal abnormalities [1], it remains a

major challenge in orthopedic surgery. The autologous bone graft with optimal biological properties is still the gold standard treatment; however, this is associated with significant problems, such as limited supply and donor-site morbidity [2]. The bone tissue engineering approach has provided an alternative method of bone regeneration [3-5], and 3-dimensional (3-D) printed scaffolds have been extensively studied for the use in tissue engineering [6]. Using this method, the 3-D scaffolds provide a template for seeded cells to stimulate cell proliferation and differentiation, meanwhile providing an interconnected pore structure to allow nutrients to penetrate into the scaffolds, resulting in the regeneration of bone defects [7, 8].

Recently, there has been increasing interest in the use of borosilicate bioactive glasses (BG) as scaffold materials for bone repairing [9-11], due to their faster absorption rate compared to silicate glasses. The structure and chemistry of BG can be tailored by changing their composition or their thermal or environmental processing history [12-15]. Jia *et al.* demonstrated that bioactive glass scaffolds possessed exceptional mechanical properties and excellent osteogenic and angiogenic properties, making them good candidates for large load-bearing applications [7]. Compared with non-mesoporous bioactive glass, mesoporous bioactive glass (MBG) has significantly better effects on bone regeneration [16-18]. The MBG scaffolds are similar to the porous structure of subchondral bone, because of their highly inter-connected large pores (300-500 μm) and well-ordered mesoporous structure (5 nm). Consequently, MBG scaffolds promote greatly-enhanced attachment, spreading and proliferation of cells, resulting in high bioactivity and degradation properties, due to the improved nano-pore volume and surface area [19-21]. Several studies on MBG composite scaffolds used for the repair of bone defects have been reported. For example, Wu *et al.* showed that a composite of multifunctional nano-diamond and PLGA materials had good mechanical properties and increased mineralization [19]. Another recent study showed that an MBG-coated poly L-lactic acid (PLLA) composite scaffold promoted cellular response, and had a remarkable ability to take up and release gentamicin sulfate [22]. Yang *et al.* reported that doped-PHBHHx composite scaffolds improved bioactivity and promoted the attachment and proliferation of hMSCs [22]. However, most of the composite scaffolds have low compressive strength, limiting their application in the repair of load-bearing bone defects.

In this study, we prepared synthetic biomedical materials based on borosilicate bioactive glass (BG)

and coated the surface of the BG scaffold with MBG by the dip-coating method. We hypothesized that the complex scaffolds with both macro- and meso-pores may have greatly improved osteogenic properties, and have excellent bioactivity, as well as achieving a comparable mechanical function to bone, making them suitable for the repair of bone defects.

Materials and methods

Fabrication of bioactive borosilicate glass (BG) scaffolds

The parent borosilicate bioactive glass (named BG, with a composition 6Na₂O, 8K₂O, 2MgO, 6SrO, 22CaO, 36B₂O₃, 18SiO₂, 2P₂O₅; mol.%) was the same as used in our previous studies [7]. BG scaffolds were fabricated using a robotic deposition device (Robo CAD 3.0, 3D Inks, Stillwater, OK, USA) according to a previously-reported method [1]. Cylinder models were loaded onto the 3-D robocasting software, and scaffolds were printed layer-by-layer through the extrusion of the paste similar to making noodles. After extrusion, scaffolds were dried in air for 24 h and then heated at 1 °C min⁻¹ to 600 °C to decompose the organic polymers before sintering at 620 °C for 2 h.

Preparation of MBG-coated bioactive glass (BG-MBG) composite scaffolds

The MBG precursor solution was prepared using nonionic block copolymer EO20PO70EO20 (P123) according to a previous report [22]. Briefly, P123 (4.0 g), tetraethyl orthosilicate (TEOS, 6.7 g), Ca(NO₃)₂·4H₂O (1.4 g), triethyl phosphate (TEP, 0.73 g), and 0.5 M HCl (1.0 g) were dissolved in ethanol (60 g) and stirred at room temperature for 1 day. Then the sintered bioactive glass scaffolds were immersed into the solution for 10 min. After they were transferred to a Petri dish, the excess solution was removed by centrifugation for 10 min at a speed of 1000 rpm and some of the ethanol was allowed to evaporate slowly at room temperature for 24 h. This coating procedure was repeated 3, 6, or 9 times, and the resulting scaffolds were named 3-MBG-BG (BG-3M), 6-MBG-BG (BG-6M), and 9-MBG-BG (BG-9M) respectively. When completely dried, the samples were extracted with anhydrous ethanol at 80°C for 24 h, in which 1 vol.% HCl (37 wt.%) was added, and the ethanol was changed every 8 h to extract as much P123 as possible.

Characterization of scaffolds

The mesoporous structure of MBG was confirmed using transmission electron microscopy (TEM) with a JEM-2010 electron microscope operated at an acceleration voltage of 200 kV, and N₂ adsorption-desorption isotherms were obtained on a Micromeritics Tristar 3020 at -196°C under continuous adsorption

conditions. The microstructure of BG-MBG composite scaffolds was observed by scanning electron microscopy (SEM, Hitachi S-4300, Tokyo, Japan).

Compressive strengths of the BG-MBG composite scaffolds were measured by uniaxial testing using a servo-hydraulic testing machine (MTS810, MTS Systems, Eden Prairie, MN, USA). Cubic blocks (3 mm × 3 mm × 3 mm) for mechanical testing were cut from the sintered cylinders of scaffolds and then subjected to surface grinding to eliminate the edge effects and obtain parallel testing surfaces. The specimens were compressed in the direction parallel to the pore channels at a cross-head speed of 0.5 mm min⁻¹. At least 20 specimens of each type of scaffold were tested to obtain statically reliable values.

Bioactivity analysis

Five samples of each type of scaffold were soaked in 50 mL simulated body fluid (SBF) solution in a rotated bath at a temperature of 37°C with shaking at 100 rpm. After 7 days, the specimens were removed, gently rinsed with distilled water, and dried overnight at a temperature of 60°C. The samples were then sputter-coated with gold, and the existence and morphology of the apatite formed on the material surface were observed using an environmental scanning electron microscope (ESEM, FEI Quanta 250, FEI, Hillsboro, OR, USA).

The SBF solutions used to soak the samples were collected to determine the ion concentrations of B and Si by inductively coupled plasma atomic emission spectroscopy (Optima 2100 DV, Perkin Elmer, Waltham, MA, USA). The change in pH values of the solution, as well as the weight losses of the dried scaffolds were examined to check the degradation properties of the samples. All data were derived from the average of five replicate samples.

Cell attachment and proliferation

Human bone marrow stromal cells (hBMSCs) were obtained from four donors who provided written informed consents. Briefly, marrow of the femoral midshaft was extracted and then suspended in minimum essential medium alpha (α-MEM) containing 10% fetal bovine serum (FBS, Hyclone, Logan, UT, USA), 100 U/mL of penicillin and 100 mg/L of streptomycin (Hyclone). Subsequently, the non-adherent cells were discarded, and when the adherent cells reached 80–90% confluence they were passaged and became passage one (P1) cells. P3 cells were used for experiments.

To examine cellular morphology, 1 × 10⁵ cells were seeded onto each scaffold in wells of a 24-well plate and incubated for 7 days, and then the samples were removed from the culture wells, rinsed with

phosphate buffered saline (PBS) and fixed with 2.5% glutaraldehyde in PBS for 1 h. The fixative was removed by washing with buffer containing 4% (w/v) sucrose in PBS and post-fixed in 1% osmium tetroxide in PBS followed by sequential dehydration in graded ethanol (50%, 70%, 90%, 95%, 100%) and hexamethyl disilazane. The specimens were coated with gold and the morphological characteristics of the attached cells were observed using SEM.

To measure cell proliferation, 1 × 10⁵ cells were seeded onto each scaffold in a 24-well plate and allowed to adhere to the scaffolds for 3 h. Medium was then added and the cells were incubated in humidified culture conditions. The proliferation of hBMSCs cultured on scaffolds was determined using the Cell Counting Kit-8 assay (CCK-8; Dojindo Molecular Technologies Inc., Kumamoto, Japan). Briefly, hBMSCs were cultured on scaffolds at an initial density of 10⁴ cells per scaffold for 1, 3 and 7 days. Subsequently, 360 μL of culture medium and 40 μL of CCK-8 solution were added to each well at each time point and incubated at 37°C for another 4 h. At the end of the incubation, 100 μL of solution was removed from each well and transferred to a fresh 96-well plate. The light absorbance of these samples was measured at 450 nm with a microplate reader (Bio-Rad 680, Bio-Rad, Hercules, CA, USA). All the results are presented as the optical density (OD) values minus the absorbance of blank wells.

Osteogenic differentiation of hBMSCs

To investigate osteogenic potential, 1 × 10⁵ cells were seeded onto each scaffold and cultured in a 24-well plate for 7 or 14 days to assess alkaline phosphatase (ALP) activity. At the predetermined time point, culture medium was decanted and the cell layer washed gently three times with PBS followed by washing once in cold 50 mM Tris buffer, and then cells were lysed in 200 μL of 0.2% Triton X-100.

Lysates were sonicated after being centrifuged at 14,000 rpm for 15 min at 4°C. Then 50 μL of supernatant was mixed with 150 μL working solution according to the manufacturer's protocol (Beyotime Institute of Biotechnology, Jiangsu, China). The conversion of *p*-nitrophenyl phosphate into *p*-nitrophenol in the presence of ALP was determined by measuring the absorbance at 405 nm with a microplate reader (Bio-Rad 680). The ALP activity was calculated from a standard curve after normalizing to the total protein content, which was determined by a Micro-BCA protein assay kit (Pierce, Rockford, IL, USA) at 570 nm with a microplate reader (Bio-Rad 680). The results are expressed in μM of *p*-nitrophenol produced per min per mg of protein.

The expression levels of osteogenesis-related

genes (runt-related transcription factor 2 (RUNX-2), osteocalcin (OCN), and collagen type I (COL1)) were measured using quantitative reverse transcription polymerase chain reaction (qRT-PCR) analysis. Typically, the cells were seeded at a density of 2×10^4 cells per scaffold, cultured for 3 or 7 days, then harvested using Trizol Reagent (Invitrogen Carlsbad, CA, USA) to extract the RNA. The obtained RNA was reverse-transcribed into complementary DNA (cDNA) using a Revert Aid First Strand cDNA Synthesis Kit (Thermo Fisher Scientific, Waltham, MA, USA) and qRT-PCR analysis was performed on an ABI Prism 7300 Thermal Cycler (Applied Biosystems, Foster City, CA, USA) using SYBR Green detection reagent. The relative expression of the genes of interest was normalized against the housekeeping gene glyceraldehyde 3-phosphate dehydrogenase (GAPDH). All samples were assayed in triplicate and independent experiments were performed three times. The relative expression was calculated using the formula: $2^{-\Delta\Delta Ct}$.

Animal experiments

All rats were provided with sterilized food and water and housed in a barrier facility under a 12-hour light/dark cycle.

All surgical procedures were conducted under general anesthesia, and postoperative analgesic care was ensured with tramadol. All efforts were made to minimize animal suffering and distress. The animals were anesthetized by intraperitoneal injection of chloral hydrate (4%, 9 mL/kg body weight) and all operations were performed under sterile conditions. Twenty-four rats were randomly allocated into the following groups: (1) BG (n = 6), (2) BG-3M (n = 6), (3) BG-6M (n = 6) and (4) BG-9M (n = 6).

For the surgical procedure as previously described [23], femoral cylindrical defects were created, which were standardized at 3 mm in diameter, penetrated internally approximately 3 mm in length, and lay above the distal epiphyseal growth plate. At 8 weeks after operation, the rats were sacrificed and femurs were harvested and fixed in a 4% paraformaldehyde solution buffered with 0.1 M phosphate solution (pH = 7.2) before further analysis.

Microcomputed tomography (micro-CT)

All the harvested specimens were examined on a micro-CT system (mCT-80, Scanco Medical AG, Bassersdorf, Switzerland) to evaluate new bone formation within the defect region. Briefly, the undecalcified samples were scanned at 18 μ m resolution. After 3-D reconstruction, bone mineral density (BMD) and bone volume fraction (BV/TV) in defect regions were used to evaluate new bone

formation using its auxiliary software [24].

Sequential fluorescent labeling

At 2, 4 and 6 weeks after operation the SD rats were intraperitoneally injected with tetracycline (TE, 25 mg/kg of body weight), alizarin red (AL, 30 mg/kg of body weight) and calcein (CA, 20 mg/kg of body weight), respectively. Then the mineralized tissue was observed by the trichromatic sequential fluorescent labeling method [25].

Histological analysis

One part of each specimen was dehydrated in ascending concentrations of alcohols from 70% to 100%, and then embedded in polymethylmethacrylate (PMMA). After hardening, the sagittal sections of the specimens were cut into 150–200 μ m thick slices using a microtome (Leica Microsystems Ltd., Wetzlar, Germany), and then glued onto a plastic support to polish to a final thickness of approximately 50 μ m. First, the sections were examined by confocal laser scanning microscopy (CLSM) (Leica) to examine fluorescent labeling, then new bone formation and mineralization were quantified at six locations of the defect site. The mean value of the six measurements was calculated to obtain average values for each group. Next, the sections were stained with van Gieson's picrofuchsin to evaluate new bone formation, with the red area representing new bone formation [26]. The area of new bone formation was evaluated quantitatively in six randomly-selected sections by Image Pro 5.0 (Media Cybernetics, Rockville, MD, USA).

Immunohistochemical (IHC) analysis

The remaining parts of each specimen were decalcified for approximately 2 weeks, then dehydrated through gradient alcohols, embedded in paraffin, and sectioned into 5 μ m thick sections. Then IHC staining of osteocalcin (OCN) was performed to evaluate osteogenesis in the specimens [27].

Statistical analysis

All the above data are presented as mean \pm standard deviation (SD). Differences between groups were calculated by one-way analysis of variance (ANOVA) and Student–Newman–Keuls post-hoc tests. The statistical analysis was conducted using SPSS 17.0 software (SPSS Inc., Chicago, IL, USA). The difference was considered significant when $P < 0.05$.

Results

Characterization of MBG and BG-MBG composite scaffolds

As indicated by the analysis of TEM micro-

graphs in Fig. 1B, the MBG powder contains highly-ordered mesoporous channels. Fig. 1A shows the N₂ adsorption-desorption isotherm of MBG powder, corresponding to pore size distributions in the powder. The results exhibited the type IV isotherm, suggesting the mesoporous structure of MBG powder. Fig. 1A also shows the pore size distribution curve of MBG, which was calculated from the desorption branches using the BJH model. The peak pore size is 3.94 nm. The results of SEM micrographs showed that the pore structure of the BG-MBG composite scaffold was quite uniform, and provided sufficient space for a large number of cells, allowing cell adhesion and ingrowth. Subtle morphological variations before and after surface-doping were observed at higher magnifications of SEM micrographs on the cross-section of the scaffold (Fig. 1C). The unitary BG scaffold had smooth walls. After MBG-dip-coating, the macroporous structure remain-

ed the same in all composite scaffolds, but the surface morphology and topography became rougher with each round of coating. A dense layer of MBG particle aggregates on the surface of the macropores was observed in the BG-MBG composite scaffold.

To quantify the effect of the MBG coating on the mechanical properties of the BG-MBG scaffolds, the compressive strength of the samples was measured. The maximum compressive strength of the four groups of scaffolds was around 32 MPa, and the MBG coating did not obviously influence the scaffold's compressive strength (Fig. 1E). In the initial degradation phase, the compressive strength of scaffold will be strong enough for weight loading, and in final phase scaffold will degrade and compressive strength degrade largely [42]. The reason of compressive strength has no significance difference might be the micro-coating layer is not thick enough to change the macro mechanical performance statistically.

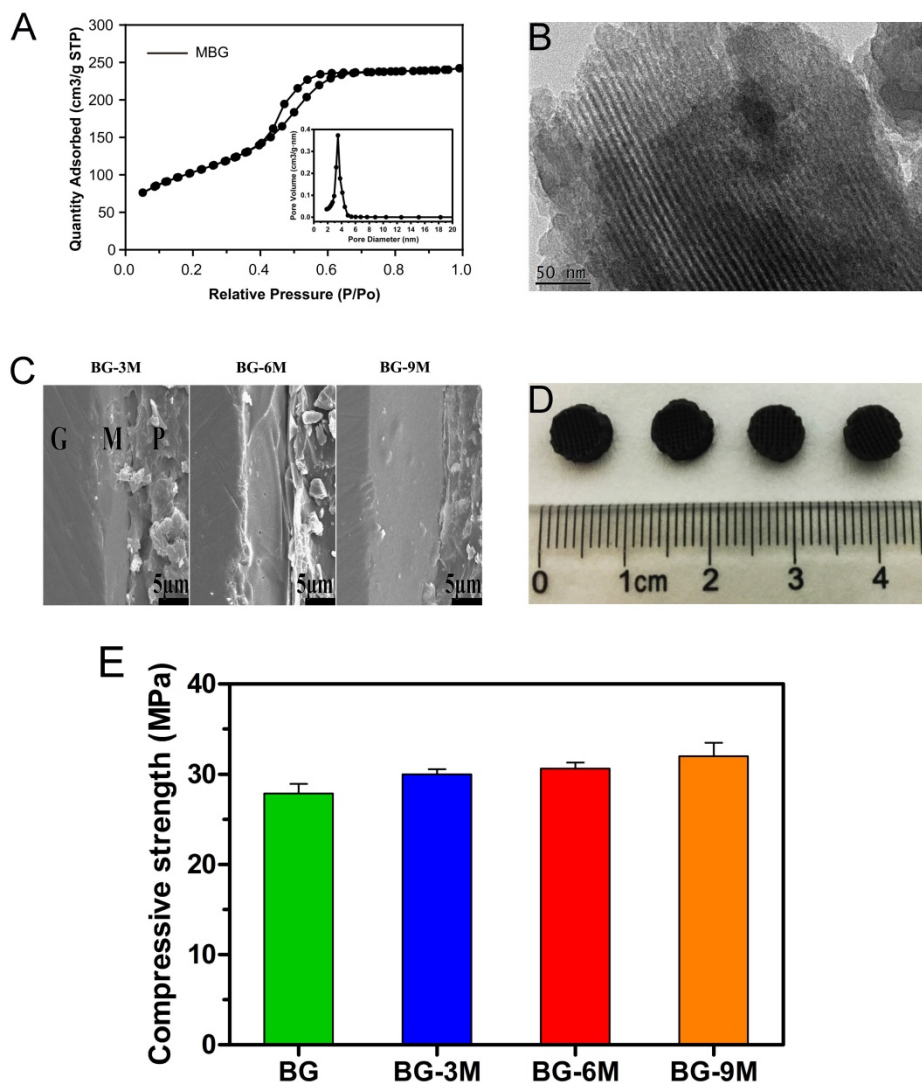


Figure 1. Characterization of MBG and BG-MBG composite scaffolds. (A) N₂ adsorption-desorption isotherms and corresponding pore size distributions of MBG, (B) TEM image of the mesopore surface in MBG, (C) SEM image showing the cross section of BG-MBG scaffolds after coating with MBG, G: glass, M: MBG, P: polymer. (D) optical images of the four scaffold groups. (E) Compressive strength comparison of the four groups of BG and BG-MBG scaffolds (n=20).

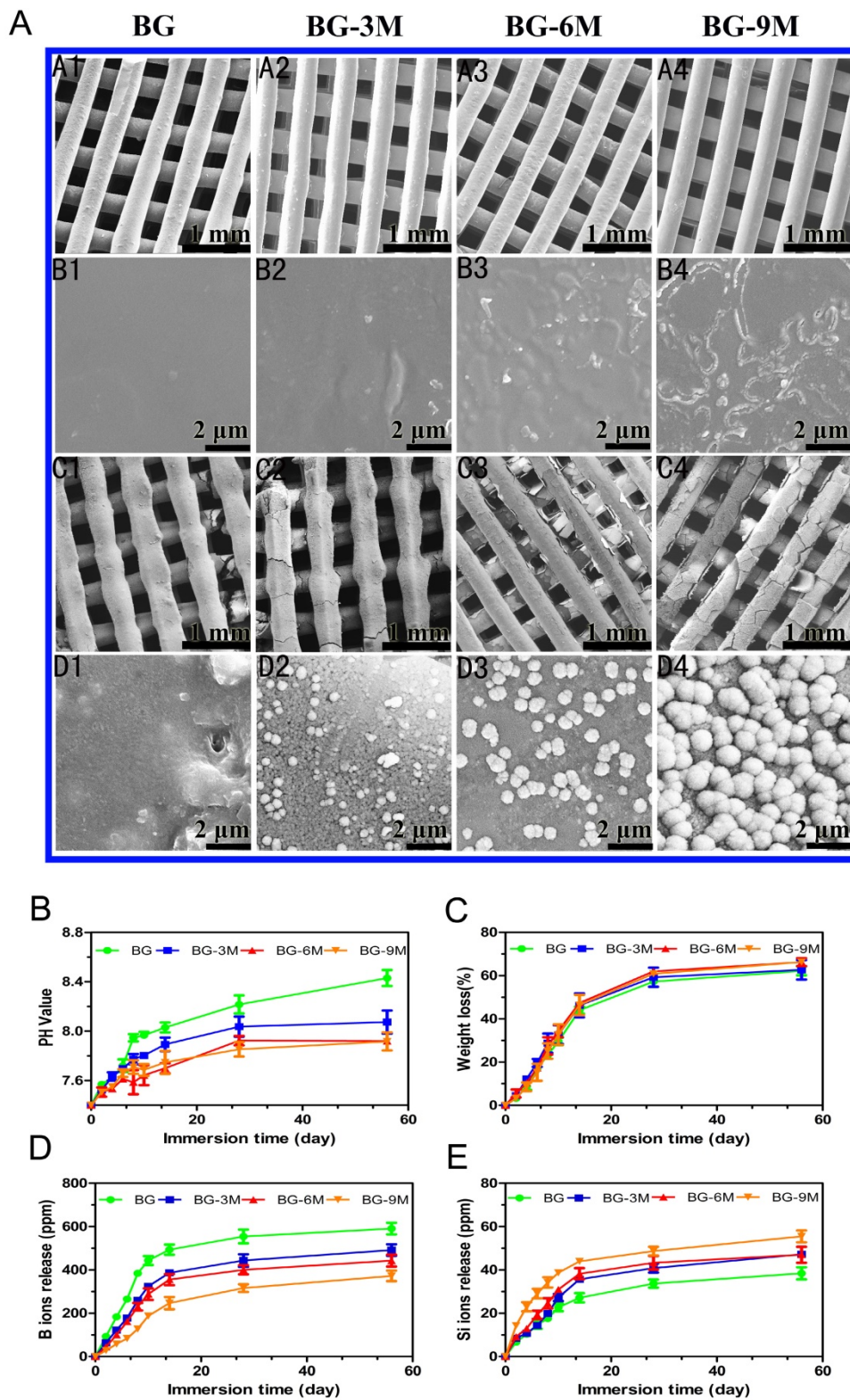


Figure 2. Apatite mineralization ability and bioactivity analysis of BG-MBG composite scaffolds. (A) SEM images (A1–B4) of BG-MBG scaffolds before being immersed in SBF, SEM images (C1–D4) of the four groups of scaffolds after being immersed in SBF for 7 days. (B) The change in the pH value and (C) weight loss for the four groups of bioactive glass scaffolds, (D) cumulative amount of B ions and (E) Si ions (E) released from the scaffolds into SBF(n=5).

Degradation and apatite mineralization ability of BG-MBG scaffolds

A study of *in vitro* bioactivity was carried out

using simulated body fluid (SBF). Surface morphologies of BG-MBG scaffolds were characterized to evaluate apatite formation after being immersed for 7 days in SBF, as shown in Fig. 2A.

No obvious differences were evident on the surface of BG scaffolds after immersion in SBF for 7 days (Fig. 2A.C1–D1). However, after immersion of BG-MBG for the same duration, an obvious difference of a hydroxyapatite layer could be observed on all the surfaces, compared to the relatively smooth surface before SBF immersion (Fig. 2A.A2–B4). With increasing content of MBG, the apatite crystalline aggregates became much denser. The flower-like particles that covered the surfaces of the BG-9M scaffolds (Fig. 2A.C4–D4) were bigger and more uniform than those that covered BG-3M (Fig. 2A.C2–D2) or BG-6M (Fig. 2A.C3–D3). Our results showed that coating of MBG onto the surface of BG scaffolds significantly enhanced their bioability in SBF, compared to BG scaffolds. Similar results were observed by Lin who studied poly (dl-lactide-co-glycolide) (PLGA) and MBG composites [24].

As shown in Fig. 2B, the pH values of the scaffolds soaked in SBF solution were changed. With increasing mass ratios of MBG, the pH values of immersed SBF solutions decreased, and showed little further decrease at the high mass ratio of MBG, indicating that the pH of the SBF did not decrease

linearly with increasing MBG. In addition, as shown in Fig. 2C, MBG could be used to tune the degradation rates of BG-MBG scaffolds, since the degradation rates of the scaffolds reduced with the increase of MBG. It is established that MBG-coating reduces the sudden release of B ions as shown in Fig 2D, and then alleviates the instant toxicity of B ions. As a result, the release of Si ions increased with the increasing mass of coated MBG (Fig. 2E).

Cellular responses to BG-MBG scaffolds

hBMSCs were cultured with scaffolds to investigate the cell compatibility of fabricated BG-MBG scaffolds. The attachment and morphology of cells on scaffolds were observed by SEM (Fig. 3). After being cultured for 7 days, hBMSCs attached to the surface of the pore struts in scaffolds, showing well-spread morphology. As determined by CCK-8 proliferation assay (Fig. 4A), all BG and BG-MBG scaffolds supported cell proliferation well; however, the proliferation rates of BG-MBG scaffolds were significantly higher than those of BG scaffolds at days 3 and 7 ($P < 0.05$), and the BG-9M group showed the best rate when compared to the others at days 3 and 7 ($P < 0.05$). ALP activity of cells cultured on scaffolds

for 7 and 14 days is shown in Fig. 4B. Similar to the cell proliferation results, cells on the BG-MBG scaffolds exhibited a significant enhancement of ALP activity compared to those on the BG scaffolds ($P < 0.05$). Cell differentiation of hBMSCs on BG and BG-MBG scaffolds was further evaluated by osteogenic potential, determined by expression of the osteogenic markers ALP, OCN and RUNX-2 at 7 and 14 days (Fig. 4C–E). The expression of these osteogenic-related genes was upregulated in cells grown on BG-MBG scaffolds compared to BG scaffolds ($P < 0.05$), indicating that the BG-MBG scaffolds could promote osteogenic differentiation.

Analysis of bone regeneration in femoral defects

Micro-CT measurement

Three-dimensional micro-CT reconstructed images show the morphology of the newly-formed bone (Fig. 5A1–D1). In the sagittal view (Fig. 5A2–D2), more newly-formed bone was observed in

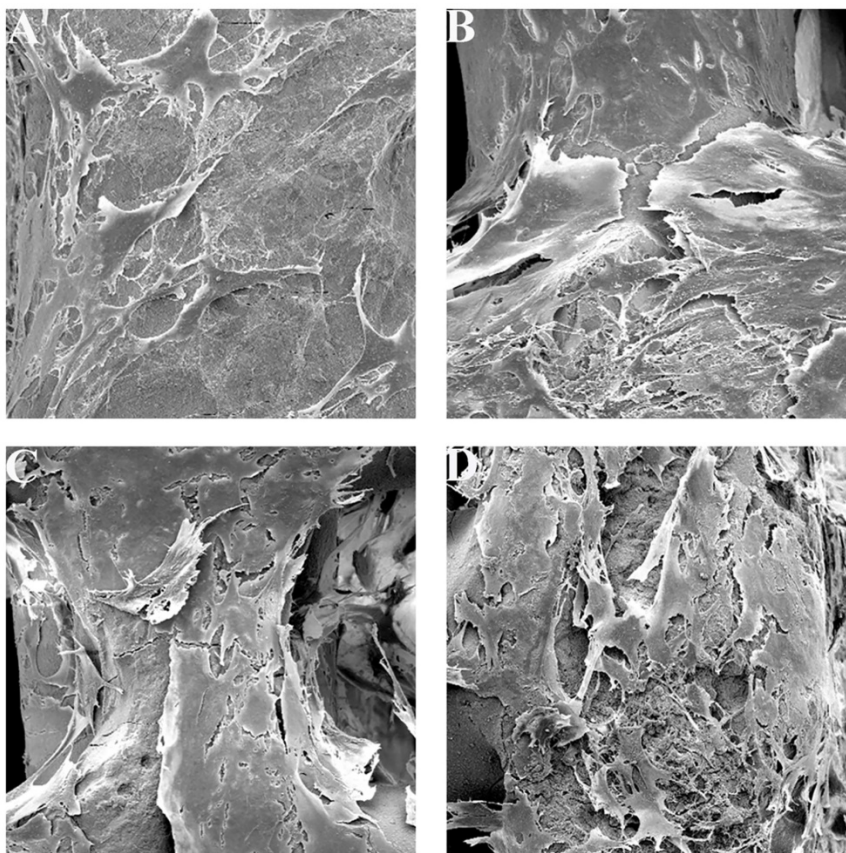


Figure 3. Cell attachment of BG-MBG composite scaffolds. SEM images showing the attachment of hBMSCs onto each of the four types of BG and BG-MBG scaffold after culturing for 7 days, A: BG, B: BG-3M, C: BG-6M, D: BG-9M ($\times 5000$).

BG-9M scaffold groups than in other groups. Quantitative analysis of the newly-formed bone was performed by the image analysis system. The local BMD was markedly higher in the BG-9M scaffold group ($0.63 \pm 0.02 \text{ g/cm}^3$) than that in the BG scaffold group ($0.13 \pm 0.02 \text{ g/cm}^3$), the BG-3M scaffold group ($0.23 \pm 0.02 \text{ g/cm}^3$) or the BG-6M scaffold group ($0.35 \pm 0.03 \text{ g/cm}^3$) ($P < 0.05$) (Fig. 5E). Moreover, the differences in BV/TV between these groups showed the same pattern (Fig. 5F). The results indicate that BG-MBG scaffolds can significantly improve bone regeneration and that BMD increases with the increasing content of MBG.

Fluorochrome labeling and histomorphometric analysis

Fluorescent labeling analysis was performed at 8 weeks. As shown in Fig. 6, new bone formation and

mineralization were analyzed at 2, 4 and 6 weeks by fluorescence labeling. At 2 weeks, the percentage of TE labeling (yellow) in the BG-9M scaffold group ($1.15 \pm 0.07\%$) was greater than that in the BG scaffold group ($0.07 \pm 0.02\%$), the BG-3M scaffold group ($0.14 \pm 0.03\%$) or the BG-6M scaffold group ($0.48 \pm 0.03\%$) ($P < 0.05$). At 4 weeks, the highest percentage of AL labeling (red) was observed in the BG-9M scaffold group ($1.71 \pm 0.21\%$), but there was also a significant difference between the BG scaffold group ($0.27 \pm 0.05\%$) and the BG-3M scaffold ($0.44 \pm 0.03\%$) and BG-6M scaffold groups ($0.60 \pm 0.06\%$) ($P < 0.05$). At 6 weeks, the percentage of CA labeling (green) in the BG-9M scaffold groups ($1.64 \pm 0.11\%$) was significantly higher than that in the BG scaffold ($0.37 \pm 0.06\%$), BG-3M scaffold ($0.53 \pm 0.04\%$) or BG-6M scaffold groups ($0.68 \pm 0.04\%$) ($P < 0.05$).

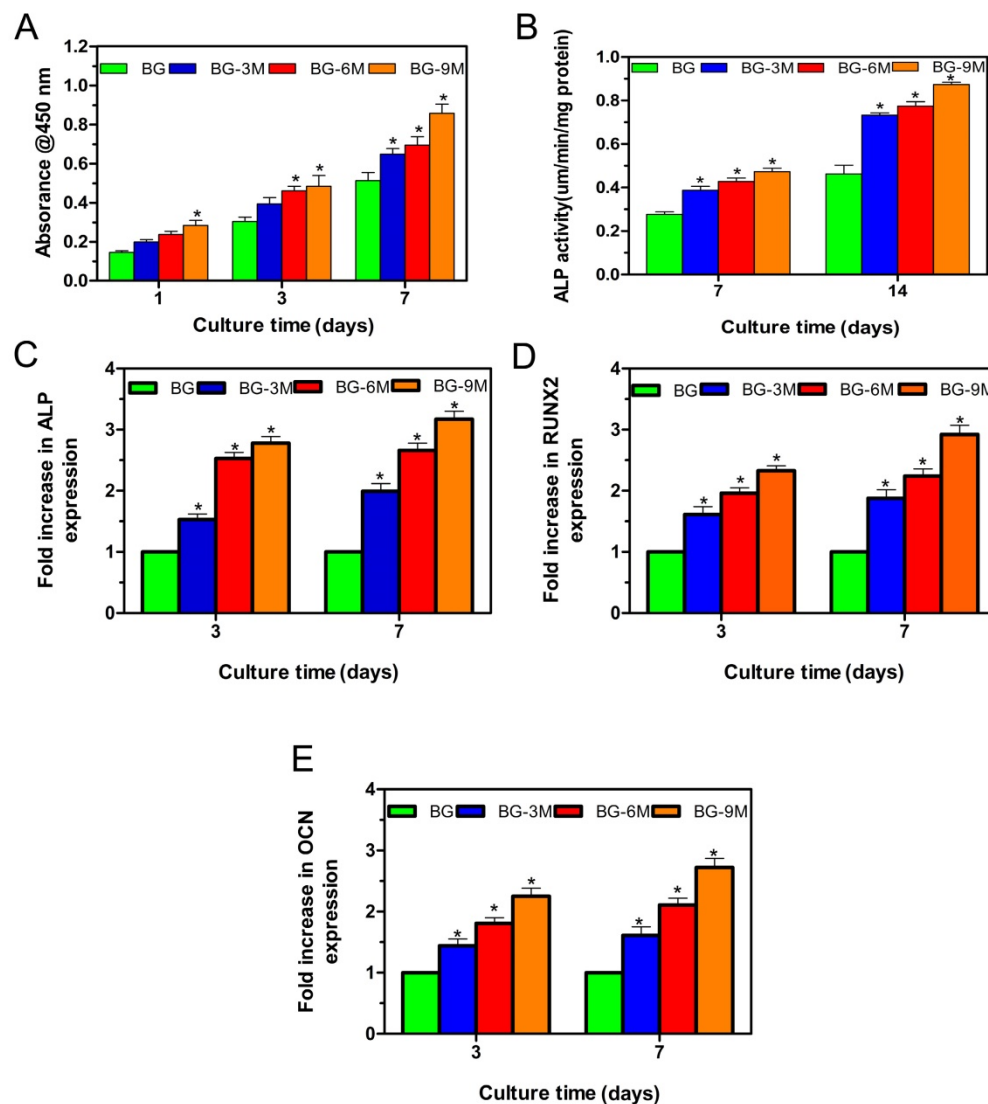


Figure 4. Cellular responses to BG-MBG composite scaffolds. (A) Quantitative analysis of the proliferation of hBMSCs cultured on the four BG and BG-MBG scaffold groups for 1, 3 and 7 days. (B) ALP activity of hBMSCs cultured for 7 and 14 days on the four BG and BG-MBG scaffold groups. The qRT-PCR analysis of the osteogenic genes ALP (C), RUNX2 (D) and OCN (E) expressed by hBMSCs cultured for 7 and 14 days on the four BG and BG-MBG scaffold groups (*indicates significant differences when compared to BG, $P < 0.05$, $n=20$).

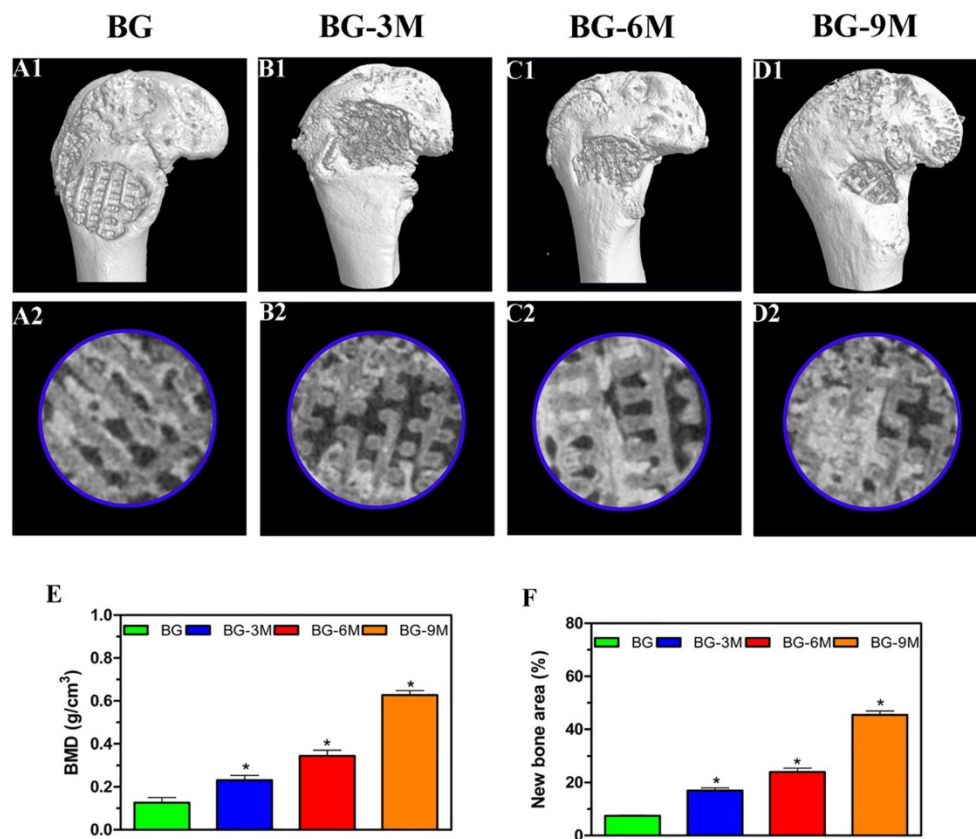


Figure 5. The results of micro-CT analysis. Representative 3D reconstruction of superficial (A1–D1) and sagittal images (A2–D2) of bone defects at 8 weeks after implantation of BG and BG-MBG scaffolds, (E) Morphometric analysis of bone mineral density (BMD) and (F) bone volume/total volume (BV/TV) by micro-CT for each group at 8 weeks (*indicates significant differences when compared to BG scaffolds, $P < 0.05$, $n = 6$).

Histological and immunohistochemical analysis

Consistent with the above results, the histological analysis of van Gieson staining of undecalcified specimens showed extensive new formation of bone in the defect areas (Fig. 7), and bone regeneration was markedly increased in the BG-9M scaffold groups ($62.67 \pm 3.39\%$), with the new bone formation area significantly greater than that in the BG scaffold ($12.33 \pm 2.58\%$), BG-3M scaffold ($22 \pm 3.46\%$) and BG-6M scaffold groups ($33 \pm 2.45\%$) ($P < 0.05$).

IHC analysis

The osteogenic marker OCN was detected by immunohistochemical staining of decalcified femurs (Fig. 8). There was virtually no obvious positive staining for OCN in the BG scaffold group, but positive brown staining for OCN was apparent in the BG-MBG groups, and obvious positive staining was found in the BG-9M scaffold groups. The analysis of bone regeneration in femoral defects indicated that BG-MBG scaffolds can significantly improve bone regeneration, which increases in line with the increasing content of MBG, results which were consistent with the previous micro-CT results.

Discussion

In this study, we have successfully fabricated novel MBG-coated 3-D printed scaffolds. Bioactive borosilicate glasses (BG) with certain compositions were used as scaffold materials and fabricated into 3-D constructs. BG was chosen because of its excellent workability, and then MBG was coated onto the surface of the scaffolds. Using this system, users can precisely control the structure of the scaffolds, as well as the pore size and morphology of the scaffolds by the 3-D printing technique. A scaffold can be produced with symmetrical macroporous struts and mesoporous interfaces, when 3-D printing and surface coating are used together, since the P123, a template agent gave the ordered mesopores in the coatings. Macroporous-mesoporous composite scaffolds tend to have excellent pore interconnectivity to give cells opportunities for attachment, migration and affinity, and provide a platform for transportation of nutrients and metabolic waste and bone ingrowth into scaffolds [22]. After MBG-coating, the macroporous structure had not been changed in any of the composite scaffolds, but the surface morphology and topography became rougher with increasing rounds

of coating. A dense layer of MBG particles aggregated on the surface of the BG-9M scaffolds.

Higher strength is essential for scaffolds used for implantation into femoral defects, to ensure higher survival rates and help carry the load after

implantation [15, 28]. Our results of compressive strength measurements demonstrated that the mechanical performance of BG-MBG scaffolds was obviously superior to that of HA or β -TCP ceramic constructs [43] (Fig. 1E).

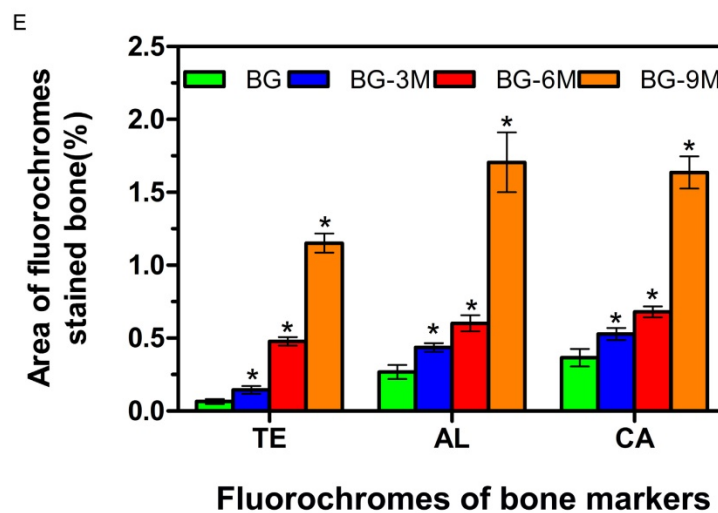
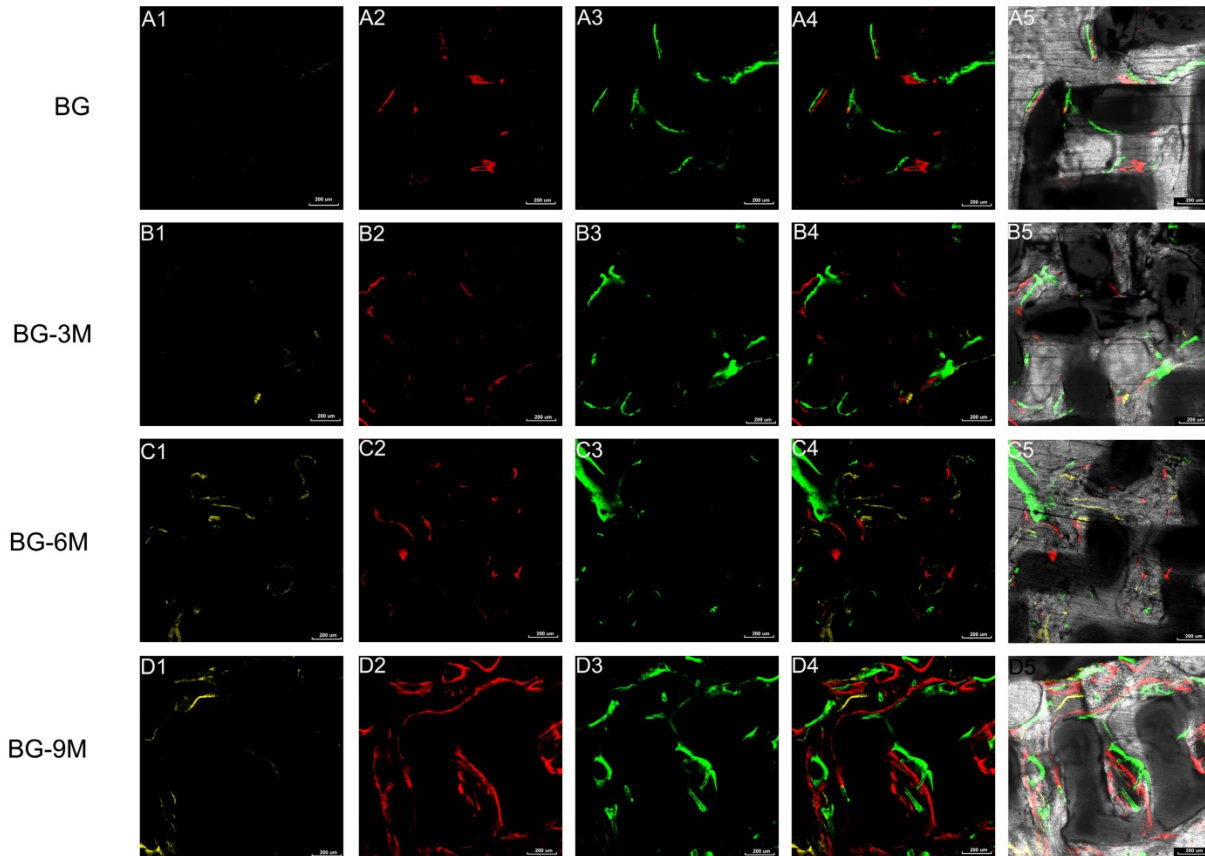


Figure 6. Fluorochrome labeling analysis. The images (A1–D1) in yellow represent labeling with tetracycline (TE), the images (A2–D2) in red represent alizarin red (AL), and the images (A3–D3) in green represent calcein (CA) indicating bone formation and mineralization at 2, 4 and 6 weeks after operation, respectively. (A4–D4): merged images of the three fluorochromes, (A5–D5): merged images of the three fluorochromes together with a bright field confocal laser microscope image; (E) The percentage of TE, AL and CA staining for each group assessed at week 8 after implantation by histomorphometric analysis. (*indicates significant differences when compared to BG scaffolds, $P < 0.05$, $n = 6$), Scale bar: 200 μ m).

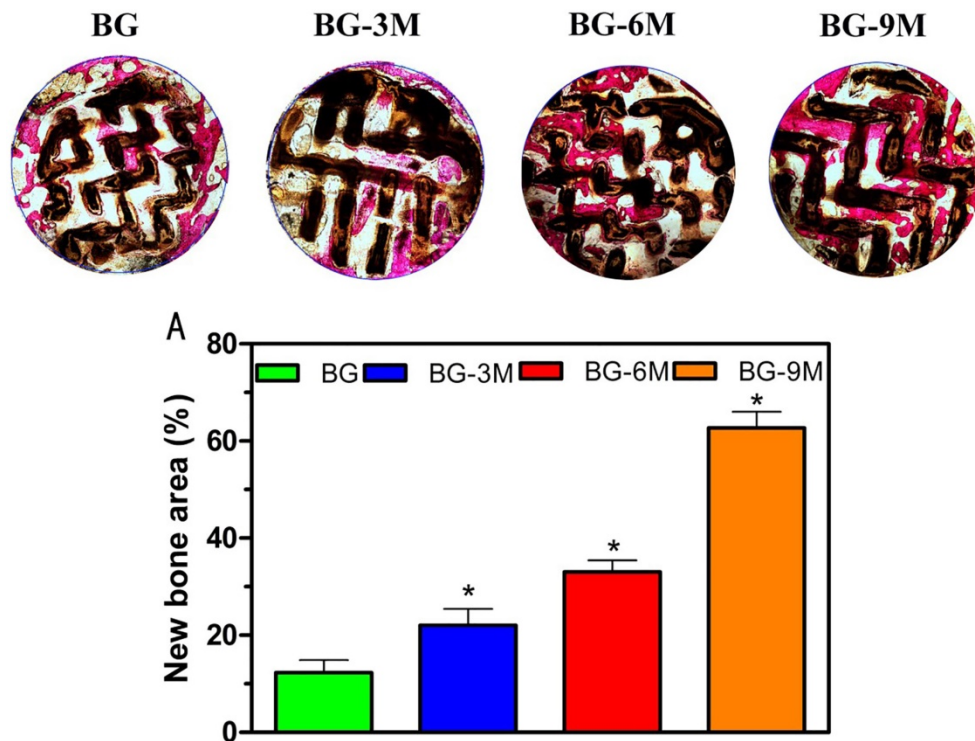


Figure 7. Histological analysis. The un-decalcified specimens were sectioned and stained with van Gieson's picrofuchsin. The area of newly-formed bone is shown in red. (A) The percentage of new bone area was assessed at 8 weeks after implantation by histomorphometric analysis ($\times 40$) (*indicates significant differences when compared to BG scaffolds, $P < 0.05$, $n = 6$).

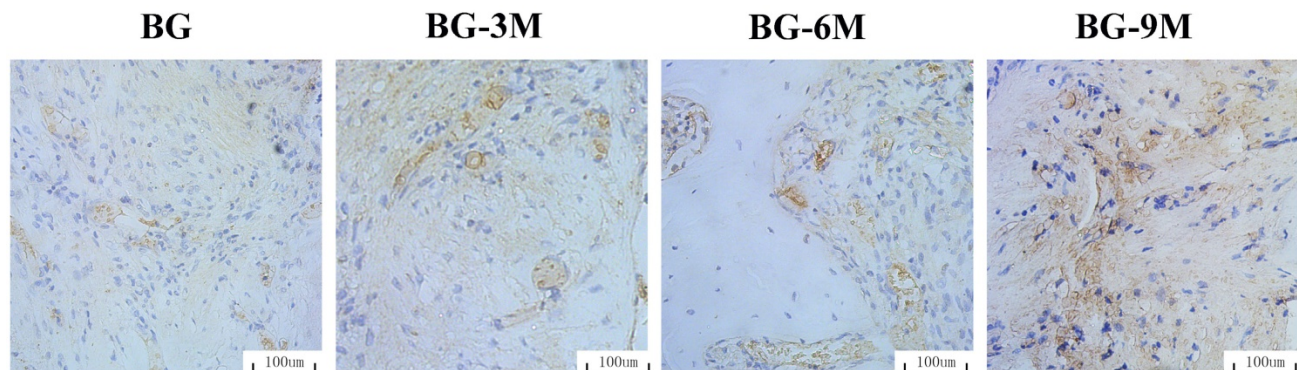


Figure 8. Immunohistochemical analysis. OCN was used to evaluate osteogenesis in femoral specimens after implantation of scaffolds. The brown color represents positive staining of OCN ($\times 200$).

The degradation and apatite mineralization ability of biomaterials in SBF is useful for investigating the bone bioactivity of this type of materials *in vivo* [29]. Furthermore, the apatite that forms on the surface of biomaterials possesses the capacity to improve the adsorption of proteins, such as osteonectin, fibronectin and vitronectin, and enhance osteoblastic activity, including cell attachment, proliferation and differentiation [30]. In this study, an apatite layer could be observed deposited on the surfaces of BG-MBG scaffolds after soaking in SBF for 3 days. The results indicated that BG-MBG scaffolds had good apatite-forming bioactivity with increasing levels of MBG. A previous study demonstrated that a

high surface area of MBG materials induced high chemical reactivity, and thereby resulted in good bone-forming bioactivity of MBG materials [1]. Moreover, B and Si ions are reported to give rise to both intracellular and extracellular responses at the interface of the glass with its cellular environment [31]. Faster *in vitro* degradation of borosilicate compared to silicate glasses has also been reported [32-34], suggesting a faster ion release rate along with glass degradation. As shown in Fig. 2D-E, there were obvious characteristic peaks of B and Si elements after SBF immersion. Although the fast release of ions from borosilicate glasses has been reported, reflected in an decrease in pH of the solution *in vitro*, this decrease

did not impact the biological performance of these glasses in a dynamic *in vivo* system [34, 35]. The results of our study are consistent with the above reports, and the results showed that with the increasing MBG, the degradation rates of scaffolds were slowed down. A thick coating would lead to a lower degradation rate of the scaffold with reduced ion release and exchange.

Generally, the proliferation and differentiation of cells are the important steps that occur before bone mineralization, and the fundamental processes of cell proliferation, differentiation and function are governed by the interaction of cells with their substrate [20, 22]. In this study, cell proliferation, ALP activity and osteogenic gene expression of hBMSCs cultured on BG-MBG scaffolds were investigated. The results showed that BG-MBG scaffolds stimulated the proliferation, ALP activity and osteogenesis-related gene expression of hBMSCs, increasing all these attributes with the increasing mass of MBG. We believe that the silica components, together with the roughness of the BG-MBG composite scaffolds might have contributed to these results. The results show that MBG has a higher surface area (Fig. 1A-B), and most researchers believe that this may promote cell growth, proliferation and differentiation, consistent with the results of several previous studies [19]. Previous studies also reported that the compositions of bioceramics could affect the biological response of cells due to the dissolution of ions from bioceramics [36, 37]. Studies reported that the released Ca, P and Si ions from bioactive glasses and more stable pH environments can stimulate the metabolic activity, proliferation and differentiation of osteoblasts [7, 38]. In this study, compared to the BG scaffolds, BG-MBG scaffolds released ions and stabilized the surrounding pH, creating a better microenvironment for osteogenesis, which may contribute to the enhanced adhesion, proliferation and differentiation of hBMSCs on BG-MBG scaffolds.

The role of BG-MBG scaffolds in bone regeneration *in vivo* was determined by testing their ability to repair femoral cylindrical defects in a rat model. Micro-CT quantitative analysis showed that the BG-MBG scaffolds could significantly improve osteogenesis in a calvarial defect model, but the BG-9M scaffolds were more effective. The BG-MBG scaffolds significantly enhanced new bone formation, with the efficacy increasing with increasing concentration of MBG. Histological analysis also showed that there was little newly-formed bone in the defect areas in the BG scaffold groups, whereas the BG-MBG scaffold groups significantly promoted bone formation, and in the BG-9M scaffolds, the new bone covered most of the defect areas, and the results were

consistent with the micro-CT findings. OCN is a common marker used in studies of osteogenic differentiation [39-41], and the results of immunohistochemical staining showed that there was only a small amount of positive staining for OCN in the defect areas of the BG scaffold group, but more positive staining for OCN in the BG-MBG scaffolds which increased with increasing MBG concentration. MBG has been shown to enhance bone-forming bioactivity, degradation and drug delivery ability [1, 5], therefore, we coated MBG onto the BG scaffolds to create a bioactive material that stimulated bone regeneration. Although the osteogenic effects of BG-MBG scaffolds are effective, the underlying biological mechanisms are not understood, we will study the underlying biological mechanisms in future studies.

In order to apply to clinical as soon as possible, once getting the approval of relevant departments, we will immediately carry out the clinical trial to transplant materials to bone defects by surgical operation.

Conclusions

In summary, BG-MBG scaffolds have been successfully fabricated by a 3-D printing technique. The results showed that BG-MBG scaffolds possessed ordered mesopores and regular macropores, as well as exhibiting good biodegradability and stimulating hBMSC proliferation and osteogenic differentiation. In *in vivo* studies, the results showed that BG-MBG scaffolds could significantly enhance new bone formation in both inner and peripheral scaffolds in defects without the presence of growth factors or stem cells. Therefore, BG-MBG scaffolds demonstrated excellent osteoinductive and osteogenic properties and will be appealing candidates for bone defect repair.

Abbreviations

bioactive borosilicate glass: BG
Quantitative reverse transcription polymerase chain reaction: qRT-PCR
human bone marrow stromal cells: hBMSCs
microcomputed tomography: micro-CT
immunohistochemical: IHC
mesoporous bioactive glass: MBG
alkaline phosphatase: ALP
Osteocalcin: OCN

Acknowledgements

The authors gratefully acknowledge the support of the National Natural Science Foundation of China (No.81601886, 51672191, 81371938, 51372170, 81572150, 81572105 and 81572178).

Ethics approval and consent to participate

Animal experiments were approved by the Research Ethics Committee at Shanghai Sixth People's Hospital affiliated to Shanghai Jiao Tong University. All animal experiments were conducted in accordance with the guidelines of the Research Ethics Committee of the sixth People's Hospital, Shanghai Jiao Tong University, and the guide for the Care and Use of Laboratory Animals.

Availability of data and material

All data generated or analyzed during this study are included in this published article.

Authors' contributions

Wenhai Huang and Shichang Zhao designed the experiments. Xin Qi, Hui Wang, Yadong Zhang and Libin Pang carried out in vitro experiments. Xin Qi and Deping Wang carried out in vivo animal experiments. Xin Qi, Hui Wang and Changqing Zhang prepared the manuscript. Wenhai Huang provided overall intellectual guidance and was the principal investigator of this group.

Competing Interests

The authors have declared that no competing interest exists.

References

- [1] Zhao S, Zhang J, Zhu M, Zhang Y, Liu Z, Tao C, et al. Three-dimensional printed strontium-containing mesoporous glass scaffolds for repairing rat critical-sized calvarial defects. *Acta biomaterialia*. 2015;12:270-80.
- [2] De Long WG, Jr., Einhorn TA, Koval K, McKee M, Smith W, Sanders R, et al. Bone grafts and bone graft substitutes in orthopaedic trauma surgery. A critical analysis. *The Journal of bone and joint surgery American volume*. 2007;89:649-58.
- [3] Chao PH, Grayson W, Vunjak-Novakovic G. Engineering cartilage and bone using human mesenchymal stem cells. *Journal of orthopaedic science : official journal of the Japanese Orthopaedic Association*. 2007;12:398-404.
- [4] Pioletti DP, Montjovent MO, Zambelli PY, Applegate L. Bone tissue engineering using foetal cell therapy. *Swiss medical weekly*. 2007;137 Suppl 155:86S-95.
- [5] Wu C, Zhou Y, Fan W, Han P, Chang J, Yuen J, et al. Hypoxia-mimicking mesoporous bioactive glass scaffolds with controllable cobalt ion release for bone tissue engineering. *Biomaterials*. 2012;33:2076-85.
- [6] Hoppe A, Jokic B, Janackovic D, Fey T, Greil P, Romeis S, et al. Cobalt-releasing 1393 bioactive glass-derived scaffolds for bone tissue engineering applications. *ACS applied materials & interfaces*. 2014;6:2865-77.
- [7] Jia W, Lau GY, Huang W, Zhang C, Tomsia AP, Fu Q. Bioactive Glass for Large Bone Repair. *Advanced healthcare materials*. 2015;4:2842-8.
- [8] Yang S, Xu S, Zhou P, Wang J, Tan H, Liu Y, et al. Siliceous mesostructured cellular foams/poly(3-hydroxybutyrate-co-3-hydroxyhexanoate) composite biomaterials for bone regeneration. *International journal of nanomedicine*. 2014;9:4795-807.
- [9] Zhang W, Zhao F, Huang D, Fu X, Li X, Chen X. Strontium-Substituted Submicrometer Bioactive Glasses Modulate Macrophage Responses for Improved Bone Regeneration. *ACS applied materials & interfaces*. 2016;8:30747-58.
- [10] Xiao W, Zaeem MA, Bal BS, Rahaman MN. Creation of bioactive glass (13-93) scaffolds for structural bone repair using a combined finite element modeling and rapid prototyping approach. *Materials science & engineering C, Materials for biological applications*. 2016;68:651-62.
- [11] Liu X, Rahaman MN, Hilmas GE, Bal BS. Mechanical properties of bioactive glass (13-93) scaffolds fabricated by robotic deposition for structural bone repair. *Acta biomaterialia*. 2013;9:7025-34.
- [12] Rahaman MN, Day DE, Bal BS, Fu Q, Jung SB, Bonewald LF, et al. Bioactive glass in tissue engineering. *Acta biomaterialia*. 2011;7:2355-73.

- [13] Fu Q, Saiz E, Rahaman MN, Tomsia AP. Bioactive glass scaffolds for bone tissue engineering: state of the art and future perspectives. *Materials science & engineering C, Materials for biological applications*. 2011;31:1245-56.
- [14] Fu Q, Rahaman MN, Bal BS, Brown RF, Day DE. Mechanical and in vitro performance of 13-93 bioactive glass scaffolds prepared by a polymer foam replication technique. *Acta biomaterialia*. 2008;4:1854-64.
- [15] Fu Q, Saiz E, Tomsia AP. Direct ink writing of highly porous and strong glass scaffolds for load-bearing bone defects repair and regeneration. *Acta biomaterialia*. 2011;7:3547-54.
- [16] Garcia A, Izquierdo-Barba I, Colilla M, de Laorden CL, Vallet-Regi M. Preparation of 3-D scaffolds in the SiO₂-P₂O₅ system with tailored hierarchical meso-macroporosity. *Acta biomaterialia*. 2011;7:1265-73.
- [17] Yan X, Huang X, Yu C, Deng H, Wang Y, Zhang Z, et al. The in-vitro bioactivity of mesoporous bioactive glasses. *Biomaterials*. 2006;27:3396-403.
- [18] Vallet-Regi M, Balas F, Arcos D. Mesoporous materials for drug delivery. *Angewandte Chemie*. 2007;46:7548-58.
- [19] Wu C, Ramaswamy Y, Zhu Y, Zheng R, Appleyard R, Howard A, et al. The effect of mesoporous bioactive glass on the physicochemical, biological and drug-release properties of poly(DL-lactide-co-glycolide) films. *Biomaterials*. 2009;30:2199-208.
- [20] Li X, Shi J, Dong X, Zhang L, Zeng H. A mesoporous bioactive glass/polycaprolactone composite scaffold and its bioactivity behavior. *Journal of biomedical materials research Part A*. 2008;84:84-91.
- [21] Wu C, Zhang Y, Zhou Y, Fan W, Xiao Y. A comparative study of mesoporous glass/silk and non-mesoporous glass/silk scaffolds: physicochemistry and in vivo osteogenesis. *Acta biomaterialia*. 2011;7:2229-36.
- [22] Yang S, Wang J, Tang L, Ao H, Tan H, Tang T, et al. Mesoporous bioactive glass doped-poly (3-hydroxybutyrate-co-3-hydroxyhexanoate) composite scaffolds with 3-dimensionally hierarchical pore networks for bone regeneration. *Colloids and surfaces B, Biointerfaces*. 2014;116:72-80.
- [23] Cheng N, Wang Y, Zhang Y, Shi B. The osteogenic potential of mesoporous bioglasses/silk and non-mesoporous bioglasses/silk scaffolds in ovariectomized rats: in vitro and in vivo evaluation. *PLoS one*. 2013;8:e81014.
- [24] Qi X, Huang Y, Han D, Zhang J, Cao J, Jin X, et al. Three-dimensional poly (epsilon-caprolactone)/hydroxyapatite/collagen scaffolds incorporating bone marrow mesenchymal stem cells for the repair of bone defects. *Biomedical materials*. 2016;11:025005.
- [25] Zhang J, Guan J, Qi X, Ding H, Yuan H, Xie Z, et al. Dimethylxaloylglycine Promotes the Angiogenic Activity of Mesenchymal Stem Cells Derived from iPSCs via Activation of the PI3K/Akt Pathway for Bone Regeneration. *International journal of biological sciences*. 2016;12:639-52.
- [26] Lin K, Xia L, Li H, Jiang X, Pan H, Xu Y, et al. Enhanced osteoporotic bone regeneration by strontium-substituted calcium silicate bioactive ceramics. *Biomaterials*. 2013;34:10028-42.
- [27] Yin W, Qi X, Zhang Y, Sheng J, Xu Z, Tao S, et al. Advantages of pure platelet-rich plasma compared with leukocyte- and platelet-rich plasma in promoting repair of bone defects. *Journal of translational medicine*. 2016;14:73.
- [28] Fu Q, Huang W, Jia W, Rahaman MN, Liu X, Tomsia AP. Three-dimensional visualization of bioactive glass-bone integration in a rabbit tibia model using synchrotron X-ray microcomputed tomography. *Tissue engineering Part A*. 2011;17:3077-84.
- [29] Loty C, Sautier JM, Boulekbache H, Kokubo T, Kim HM, Forest N. In vitro bone formation on a bone-like apatite layer prepared by a biomimetic process on a bioactive glass-ceramic. *Journal of biomedical materials research*. 2000;49:423-34.
- [30] Yan X, Yu C, Zhou X, Tang J, Zhao D. Highly ordered mesoporous bioactive glasses with superior in vitro bone-forming bioactivities. *Angewandte Chemie*. 2004;43:5980-4.
- [31] Hench LL, Polak JM. Third-generation biomedical materials. *Science*. 2002;295:1014-7.
- [32] Liu X, Rahaman MN, Day DE. Conversion of melt-derived microfibrillar borate (13-93B3) and silicate (4555) bioactive glass in a simulated body fluid. *Journal of materials science Materials in medicine*. 2013;24:583-95.
- [33] Fu Q, Rahaman MN, Bal BS, Kuroki K, Brown RF. In vivo evaluation of 13-93 bioactive glass scaffolds with trabecular and oriented microstructures in a subcutaneous rat implantation model. *Journal of biomedical materials research Part A*. 2010;95:235-44.
- [34] Fu Q, Rahaman MN, Fu H, Liu X. Silicate, borosilicate, and borate bioactive glass scaffolds with controllable degradation rate for bone tissue engineering applications. I. Preparation and in vitro degradation. *Journal of biomedical materials research Part A*. 2010;95:164-71.
- [35] Kanczler JM, Oreffo RO. Osteogenesis and angiogenesis: the potential for engineering bone. *European cells & materials*. 2008;15:100-14.
- [36] Silver IA, Deas J, Erecinska M. Interactions of bioactive glasses with osteoblasts in vitro: effects of 4555 Bioglass, and 58S and 77S bioactive glasses on metabolism, intracellular ion concentrations and cell viability. *Biomaterials*. 2001;22:175-85.
- [37] Valerio P, Pereira MM, Goes AM, Leite MF. The effect of ionic products from bioactive glass dissolution on osteoblast proliferation and collagen production. *Biomaterials*. 2004;25:2941-8.
- [38] Xynos ID, Edgar AJ, Buttery LD, Hench LL, Polak JM. Gene-expression profiling of human osteoblasts following treatment with the ionic products of Bioglass 4555 dissolution. *Journal of biomedical materials research*. 2001;55:151-7.

- [39] Karsenty G. Transcriptional control of skeletogenesis. Annual review of genomics and human genetics. 2008;9:183-96.
- [40] Nakashima K, de Crombrughe B. Transcriptional mechanisms in osteoblast differentiation and bone formation. Trends in genetics : TIG. 2003;19:458-66.
- [41] Sinha KM, Zhou X. Genetic and molecular control of osterix in skeletal formation. Journal of cellular biochemistry. 2013;114:975-84.
- [42] Fu H, Fu Q, Zhou N, et al. In vitro evaluation of borate-based bioactive glass scaffolds prepared by a polymer foam replication method[J]. Materials Science & Engineering C, 2009, 29(7):2275-2281.
- [43] Rahaman M N, Xiao W, Huang W. Review - bioactive glass implants for potential application in structural bone repair[J]. Biomedical Glasses, 2017, 3(1).